

Provided for non-commercial research and education use.
Not for reproduction, distribution or commercial use.



(This is a sample cover image for this issue. The actual cover is not yet available at this time.)

This article appeared in a journal published by Elsevier. The attached copy is furnished to the author for internal non-commercial research and education use, including for instruction at the authors institution and sharing with colleagues.

Other uses, including reproduction and distribution, or selling or licensing copies, or posting to personal, institutional or third party websites are prohibited.

In most cases authors are permitted to post their version of the article (e.g. in Word or Tex form) to their personal website or institutional repository. Authors requiring further information regarding Elsevier's archiving and manuscript policies are encouraged to visit:

<http://www.elsevier.com/copyright>



Contents lists available at SciVerse ScienceDirect

Remote Sensing of Environment

journal homepage: www.elsevier.com/locate/rse

An integrated analysis of aerosol above clouds from A-Train multi-sensor measurements

Hongbin Yu^{a,b,*}, Yan Zhang^{c,b}, Mian Chin^d, Zhaoyan Liu^{e,f}, Ali Omar^f, Lorraine A. Remer^b, Yuekui Yang^{g,b}, Tianle Yuan^{h,b}, Jialong Zhangⁱ

^a Earth System Science Interdisciplinary Center, University of Maryland, College Park, MD, USA

^b Climate and Radiation Laboratory, NASA Goddard Space Flight Center, Greenbelt, MD, USA

^c Goddard Earth Sciences Technology and Research, Morgan State University, Baltimore, MD, USA

^d Atmospheric Chemistry and Dynamics Laboratory, NASA Goddard Space Flight Center, Greenbelt, MD, USA

^e National Institute of Aerospace, Hampton, VA, USA

^f NASA Langley Research Center, Hampton, VA, USA

^g Goddard Earth Sciences Technology and Research, Universities Space Research Association, Columbia, MD, USA

^h Joint Center for Earth Systems Technology, University of Maryland, Baltimore County, Baltimore, MD, USA

ⁱ Department of Atmospheric Science, University of North Dakota, Grand Forks, ND, USA

ARTICLE INFO

Article history:

Received 10 August 2011

Received in revised form 27 November 2011

Accepted 12 January 2012

Available online xxxx

Keywords:

Aerosols

Clouds

ABSTRACT

Quantifying above-cloud aerosol can help improve the assessment of aerosol intercontinental transport and climate impacts. In this study we conduct an integrated analysis of aerosols above clouds by using multi-sensor A-Train measurements, including above-cloud aerosol optical depth at 532 nm (AOD₅₃₂) from CALIPSO lidar, the UV aerosol index (AI) from OMI, and cloud fraction and cloud optical depth (COD) from MODIS. The analysis of Saharan dust outflow and Southwest African smoke outflow regions shows that the above-cloud AOD correlates positively with AI in an approximately linear manner, and that the AOD₅₃₂/AI ratio decreases with increasing COD. The dependence of AOD₅₃₂/AI ratio on COD doesn't depend on aerosol type when potential biases in the CALIOP AOD measurements are empirically accounted for. Our results may suggest the potential of combining OMI AI and MODIS cloud measurements to empirically derive above-cloud AOD with a spatial coverage much more extensive than CALIPSO measurements, which needs to be further explored in the future.

© 2012 Elsevier Inc. All rights reserved.

1. Introduction

Quantifying above-cloud aerosol can help improve the assessment of aerosol intercontinental transport and climate impacts (Schulz et al., 2006; Yu et al., 2008). Aerosol intercontinental transport is often associated with cloud systems. Aerosols produced from source regions in the atmospheric boundary layer are pumped up to the free troposphere by convection systems. Such elevated aerosol layers can be transported above low clouds from one continent to others. Absorbing aerosols, such as those from biomass burning, dust outbreaks, industrial activities, and volcanic eruptions, when lifted above clouds could exert a positive direct radiative forcing at the top of atmosphere (Abel et al., 2005; Chand et al., 2009). The increase of radiative heating or atmospheric stratification resulting from the above-cloud aerosol absorption could also influence the formation and evolution of clouds (Johnson et al., 2004; Wilcox, 2010). However, assessing these aerosol impacts remains challenging because of the scarcity of measurements and the large uncertainties in model

simulations of above-cloud aerosols (Schulz et al., 2006; Textor et al., 2006; Yu et al., 2006).

Large-scale measurements of aerosol above clouds had been generally unexplored until very recently when the A-Train, a constellation of several satellites carrying a suite of active and passive sensors with enhanced capabilities emerged (Stephens et al., 2002). Although the majority of aerosol satellite remote sensing has been confined to cloud-free scenes (Kahn et al., 2005; Remer et al., 2005), there are now some capabilities of observing aerosols above clouds. Active sensors such as the Cloud-Aerosol Lidar with Orthogonal Polarization (CALIOP) onboard the Cloud-Aerosol Lidar and Infrared Pathfinder Satellite Observation (CALIPSO) satellite can measure aerosol backscatter and infer extinction profiles in both cloud-free and cloudy conditions (Chand et al., 2008; Winker et al., 2010). Several passive sensors also can measure columnar properties of aerosols above clouds, because the presence of aerosols can significantly modify some attributes of radiances reflected by underlying clouds. For example, smoke and dust that are absorptive in ultraviolet (UV) wavelengths interact with scattered radiation by air molecules and cloud droplets, altering the spectral contrast of the backscattered UV (BUV) radiation. Several sensors, such as the Ozone Monitoring Instrument (OMI), the Total Ozone Mapping Spectrometer (TOMS),

* Corresponding author at: NASA GSFC Code 613, Greenbelt, MD 20771, USA. Tel.: +1 301 614 6209; fax: +1 301 614 6307.

E-mail address: Hongbin.Yu@nasa.gov (H. Yu).

the Global Ozone Monitoring Experiment (GOME), and the Scanning Imaging Absorption Spectrometer for Atmospheric Chartography (SCIAMACHY), have been measuring UV-absorbing aerosols in both cloud-free and cloud-contaminated scenes using an aerosol index (AI) (Ahn et al., 2008; de Graaf et al., 2005, 2007; Herman et al., 1997; Hsu et al., 1999, 2003; Torres et al., 2007). A positive value of AI indicates the presence of an elevated dust or smoke layer, while zero or small negative AI indicates scattering aerosol and/or clouds. Most recently, an algorithm of retrieving above-cloud AOD and cloud optical depth from OMI has been developed (Torres et al., in press). Aerosols can also significantly affect the polarized light reflected by underlying clouds in certain scattering-angle ranges, which constitutes a basis for retrieving above-cloud aerosol properties using multiangle polarization measurements from the Polarization and Directionality of Earth Reflectances (POLDER) (Waquet et al., 2009). These developments provide an unprecedented opportunity for quantifying aerosol above clouds and advancing the understanding of aerosol long-range transport and climate forcing.

The objective of this study is to examine how measurements of aerosol above clouds from different sensors correlate and/or agree. We characterize smoke and dust aerosols above clouds over the Atlantic Ocean by integrating observables of aerosol and clouds from CALIOP, OMI, and the Moderate Resolution Imaging Spectroradiometer (MODIS) onboard three A-Train satellites (CALIPSO, Aura, and Aqua, respectively). The three satellites overpass the equator within 15 min of each other, making it feasible for multi-sensor analysis. Such analysis is appealing because individual sensors are complementary to each other. While CALIOP is unique in providing retrieved profiles of aerosol backscattering and inferred extinction above clouds, such observations are substantially limited in spatial coverage because CALIOP is a nadir-view active sensor with near-zero swath (Winker et al., 2009). On the other hand, OMI with its wide swath of ~2600 km has an advantage of detecting aerosols above clouds with near-daily global coverage by means of AI (Torres et al., 2007). However, AI is not an exclusive measure of aerosol loading such as AOD because it is dependent on the strength of aerosol absorption (i.e., single-scattering albedo), the height of the aerosol layer, the brightness of the surface and clouds, and the satellite observation geometry (Torres et al., 1998). MODIS high-resolution measurements of cloud fraction and cloud optical depth (Platnick et al., 2003) also complement OMI and CALIOP observations in quantifying cloudiness and cloud reflectance. Given these complementary roles of different sensors, the AOD–AI relationship would constitute a basis for potentially developing an empirical approach to deriving above-cloud AOD from OMI and MODIS measurements with more extensive coverage than CALIOP observations.

The rest of paper is organized as follows. Section 2 describes satellite datasets, domains and analysis methodology. In Section 3, we first describe major characteristics of aerosol and clouds and then examine relationships between CALIOP above-cloud AOD and OMI AI respectively for Saharan dust outflow and Southwest African biomass burning smoke outflow over the Atlantic Ocean. Section 4 summarizes major results and discusses implications from the integrated analysis.

2. Data and methods

2.1. Datasets and domains

The datasets used in the analysis include: (1) CALIOP Level 2 Version 3.01 aerosol and cloud layer products; (2) OMI Level 2 (orbital swath, ~2600 km wide) Collection 3 UV aerosol index; and (3) MODIS/Aqua Level 2 Collection 5 cloud fraction and cloud optical depth. We focus on two regions, namely “dust outflow” and “smoke outflow” over the Atlantic Ocean, as illustrated in Fig. 1. The two regions are among those with the highest occurrence frequency of aerosol–liquid water cloud overlap (Devasthale & Thomas, 2011). Two four-month periods (from June to September, 2006 and 2007) are selected, which covers

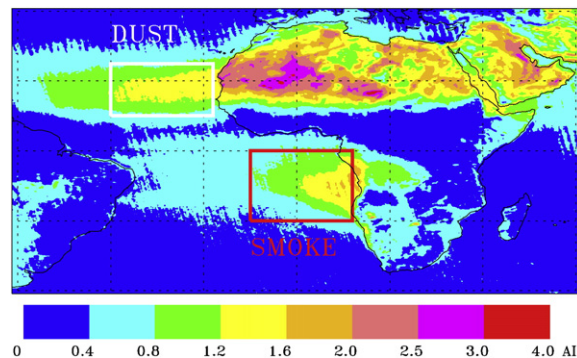


Fig. 1. Selected “dust” and “smoke” outflow regions in this analysis, which is overlaid in a map of mean OMI aerosol index averaged over June to September for 2006 and 2007.

the peak season of Saharan dust and Southwest African smoke in the dust and smoke outflow region, respectively. Smoke in the Sahel region occurs and affects the dust outflow region primarily during November–February. It is very rare that Saharan dust is transported to the smoke outflow region or Southwest African smoke is transported to the dust outflow region in the season of our investigation because the two outflow regions are separated by the inter-tropical convergence zone (ITCZ). Data after 2007 are not included in the analysis because of the unfortunate occurrence of row anomalies affecting several of OMI cross-track scenes that are co-located with CALIPSO tracks.

The CALIOP aerosol and cloud layer products report separately cloud and aerosol detection information on a 5 km horizontal grid with a vertical resolution of 30 m from the surface to about 8 km in the mid-troposphere (Winker et al., 2009, 2010). Uncertainties in CALIOP AOD are generally associated with incorrect choice of aerosol type, complete attenuation of the lidar signal when traversing thick aerosol layer, low sensitivity to the vertically dispersed layers, interference of sunlight with laser during daytime, and misclassification of cloud as aerosol or vice versa (e.g., Kittaka et al., 2011; Winker et al., 2009; Yu et al., 2010).

The OMI product has a spatial resolution varying from 13×24 km at nadir to 40×135 km at the edges of the swath (Torres et al., 2007). Uncertainties associated with AI come mainly from background noise and ground signal (Herman et al., 1997). In particular, uncorrected spectral variations in surface reflectance, particularly due to sunglint are an important source of uncertainty in positive AI (Torres et al., 2007). The single-pixel AI detection limit varies between 0.3 and 0.6 in a variety of mineral dust and smoke regions (Hsu, et al., 1999b).

The MODIS cloud optical depth is retrieved at 1 km resolution and cloud fraction is calculated at 5×5 km grid by counting the number of 1 km pixels identified as ‘cloudy’ by the cloud mask and dividing by 25, the total number of pixels in the 1 km grid box (Platnick et al., 2003). The MODIS cloud optical depth over ocean is derived primarily from the $0.86 \mu\text{m}$ radiances (Platnick et al., 2003). Thus in cases of biomass burning smoke overlying clouds, the retrieved cloud optical depth should bias low because smoke aerosol is strongly absorbing at $0.86 \mu\text{m}$. The low bias becomes greater as smoke AOD increases. Wilcox et al. (2009) found that only for scenes with OMI AI > 2 the estimated bias due to smoke absorption exceeds the instantaneous uncertainty of the retrieval. Haywood et al. (2004) suggest that the MODIS cloud optical depth in the smoke outflow region can bias low by up to 30%. On the other hand, the MODIS cloud optical depth beneath dust layers would have no significant bias because mineral dust is only weakly absorbing at $0.86 \mu\text{m}$.

2.2. Methodology

The following steps are taken to collocate and extract data from CALIOP, OMI, and MODIS. First, we identify all aerosol layers above low-level cloud (with cloud tops lower than 3 km) based on CALIOP level 2 5-km aerosol and cloud layer products.

Total AOD (at 532 nm) above cloud is calculated by adding up the identified individual layer AODs, and the aerosol centroid height (or the center of AOD) is calculated from the layer AODs such that half of the AOD value is below or above that height. For convenience we use AOD to denote aerosol optical depth in the mid-visible (at 532 nm for CALIOP or at 550 nm for MODIS) throughout the paper, unless otherwise specified. Second, for the identified CALIOP above-cloud AOD, we obtain the corresponding OMI AI and viewing geometrical parameters (solar zenith angle or SZA, viewing zenith angle or VZA, relative azimuth angle, and scattering angle) from the nearest OMI pixel that is within 20 km of the CALIOP pixel. Third, we calculate mean cloud fraction, mean cloud optical depth and its inhomogeneity over the OMI pixel from the MODIS Level 2 cloud products.

Several data screening criteria are applied. We focus on elevated UV-absorbing aerosols that produce positive AI values. Only OMI AI greater than 0.5 are selected because small AI values generally indicate large retrieval uncertainties (Torres et al., 2007). We also (1) select the path length index, which is defined as $1/\cos(\text{SZA}) + 2/\cos(\text{VZA})$, in a range of 3–7 to retain the best viewing conditions; and (2) eliminate sun glint contamination using the OMI algorithm flag (Ahn et al., 2008). For CALIOP detected aerosol layers, only those with medium and high confidence in the aerosol identification are considered, similar to Yu et al. (2010). In this study, we focus on cloudy scenes of OMI observations by selecting the average cloud fraction greater than 0.9 and cloud optical depth greater than 2 in the OMI pixels. We also focus on highly homogeneous clouds by selecting cloud inhomogeneity parameter (χ) of greater than 0.7. χ , the ratio of the logarithmic and linear average of cloud optical depth (Cahalan et al., 1994), is calculated from MODIS. It has a value between 0 and 1; the larger the value of χ , the more homogeneous the cloud. Overall these screening processes exclude about 52% and 42% of original data points in the smoke outflow and dust outflow regions, respectively.

3. Results

3.1. Aerosol and cloud characteristics in the two regions

Table 1 lists the statistics of OMI observation geometry and aerosol and cloud properties in the dust and smoke outflow regions. The mean distance between the centers of CALIOP and OMI pixels is about 10 km, which is smaller than the characteristic scale of aerosol meso-scale variations (Anderson et al., 2003). In each region, variations of

satellite observation geometry during the period are small, as characterized by small standard deviations of solar zenith angle, viewing zenith angle, and scattering angle. It is unlikely that the dependences of AI on the observation geometry (e.g., de Graaf et al., 2005) would significantly influence the interpretation of observed AOD–AI relationships as a function of cloud optical depth in each of the regions. However the solar zenith angle of 38.5° in the smoke outflow region is higher than the 25.3° in the dust outflow region, which may contribute to regional differences of AOD and AI relationships (to be discussed in Section 3.2).

The top of low-level clouds is situated at about 1.2 km in both regions. However, the cloud is optically thicker by about 30% in the smoke outflow than in the dust outflow region. The regional difference in cloud optical depth could be even larger because MODIS cloud optical depth retrieved in the visible would have been underestimated in the smoke outflow region by strong smoke absorption (Haywood et al., 2004; Wilcox et al., 2009). The stratocumulus clouds in the smoke outflow region are more homogeneous ($\chi = 0.91$) than the trade-cumulus clouds in the dust outflow region ($\chi = 0.86$), as anticipated. The high homogeneity of clouds considered in this study suggests that the regional mean of cloud optical depth can be used to calculate cloud albedo, a parameter that influences AI values, with good accuracy. The statistics show that the aerosol–cloud vertical separation (defined as difference between aerosol centroid height and cloud top height in this study) is quite similar for smoke and dust, although the dust layer on average is ~600 m thicker than the smoke layer.

While OMI observes similar AI values in the dust and smoke outflow regions (Table 1 and Fig. 1), the CALIOP above-cloud AOD₅₃₂ differs substantially. On average, AOD₅₃₂ is 130% higher in the dust outflow region (i.e., 0.32) than in the smoke outflow region (i.e., 0.14), which is consistent with CALIOP cloud-free daytime measurements. The regional and seasonal average AOD from CALIOP cloud-free observation (derived by following the data screening described in Yu et al., 2010) is 0.33 and 0.13 in the dust outflow and smoke outflow region, respectively. On the other hand, co-located MODIS/Aqua measurements (Remer et al., 2005) show AOD of about 0.31 in both regions. Note that MODIS over-ocean AOD measurements may bias high because of cloud effects and inappropriate assumptions of wind speed and aerosol microphysical properties (Zhang & Reid, 2006). Here we assess potential bias in the above values of MODIS AOD by comparing the operational MODIS AOD product with the bias-reduced MODIS AOD product in which quality check and quality assurance procedures have been implemented (Shi et al., 2011; Zhang & Reid, 2006). We found that the bias-reduced MODIS AOD is lower than the operational MODIS AOD by 19% and 30% in the dust outflow region and the smoke outflow region, respectively. By using these differences to approximate the bias associated with MODIS AOD measurements, we estimate that MODIS AOD in the dust outflow region is no more than 12% higher than that in the smoke outflow region. This regional difference is substantially lower than what CALIOP observation suggests. Our results of region-dependent CALIOP–MODIS AOD difference are generally consistent with that from an independent analysis (Kittaka et al., 2011). Although sampling introduced bias between the two sensors (due to differences in instrument resolution and sensitivity, and cloud-screening scheme, among others) could partially explain this discrepancy (Kahn et al., 2011; Zhang & Reid, 2009), much lower CALIOP AOD in the smoke region than in the dust region could be associated with underlying causes in algorithms and calibration (Kittaka et al., 2011). For example, a possible misclassification of smoke as marine aerosol in some occasions (Yu et al., 2010) would introduce substantially low bias for smoke AOD because the lidar ratio at 532 nm for smoke is more than 3 times larger than that for marine aerosol. A misclassification of heavy smoke as cloud will also bias the smoke AOD low. The regional AOD difference as seen by CALIOP will be accounted for in interpreting regional differences of AOD and AI relationship in Section 3.2.

Table 1

Statistics (mean \pm standard deviation) of OMI observation geometry, and properties of aerosols and clouds in the dust and smoke outflow regions.

Parameters		Dust outflow region	Smoke outflow region
Observation geometry	OMI solar zenith angle (SZA)	25.3 \pm 1.9°	38.5 \pm 4.6°
	OMI viewing zenith angle (VZA)	31.4 \pm 0.9°	32.7 \pm 0.9°
	OMI scattering angle	124.2 \pm 2.0°	114.3 \pm 1.6°
Cloud properties	OMI–CALIOP distance	9.8 \pm 4.1 km	9.0 \pm 4.2 km
	Cloud optical depth (COD) from MODIS	6.9 \pm 3.7	9.1 \pm 4.2
	Cloud top height (CTOP) from CALIOP	1.2 \pm 0.4 km	1.2 \pm 0.3 km
	Cloud inhomogeneity (χ) from MODIS	0.86 \pm 0.08	0.91 \pm 0.07
Aerosol properties	Aerosol Index (AI) from OMI	1.51 \pm 0.63	1.50 \pm 0.66
	Above-cloud AOD ₅₃₂ from CALIOP	0.32 \pm 0.22	0.14 \pm 0.12
	Aerosol centroid height (ACH) from CALIOP	3.5 \pm 0.6 km	3.4 \pm 0.9 km
	Aerosol layer depth from CALIOP	1.6 \pm 0.8 km	1.0 \pm 0.5 km
	Aerosol–cloud separation (= ACH – CTOP) from CALIOP	2.2 \pm 0.7 km	2.2 \pm 0.9 km

3.2. Above-cloud AOD–AI relationships and their dependence on cloud optical depth

Previous studies have examined relationships between AI and AOD from the Aerosol Robotic Network and satellites in cloud free conditions (Christopher et al., 2008; Hsu, et al., 1999b). Here we examine relationships between OMI AI and CALIOP above-cloud AOD. In our analysis, all the screened data are grouped into 5 cloud optical depth (COD) ranges: COD = 2–4, 4–6, 6–8, 8–12, and 12–20. In each COD group, the data are sorted by AI and arranged into 10 AI bins with equal number of data points. Fig. 2 shows the empirical relationships between CALIOP above-cloud AOD and OMI AI and their change with cloud optical depth in the 5-COD groups over the dust and smoke outflow regions. Note that AI values depend on the amount of intercepted radiation by the aerosol layer and hence the distance between the cloud and aerosol layer (de Graaf et al., 2005). This dependence is strong in cloud-free scenes but is weakened when clouds or bright surfaces are below the aerosol layer (de Graaf et al., 2005; Torres et al., 1998, in press). As shown in Fig. 3, the aerosol–cloud distance generally increases with AI from about 1.5 km to 2.5 km when AI increases from 0.5 to 3. This change would not yield significant change of AI, as can be inferred from a sensitivity study (de Graaf et al., 2005). Thus what is shown in Fig. 2 largely reflects the influences of AOD, COD, and aerosol absorption strength on AI. For the observed ranges of AOD and AI, CALIOP above-cloud AOD correlates positively with OMI AI in approximately linear manner, with the relationship depending on COD values. For a specific AOD a larger cloud optical depth generally corresponds to a higher aerosol index, except in some largest AI bins. The observed dependence of AI on COD is consistent with theoretical calculations that the multiple scattering of underlying cloud decks increases the amount of radiation intercepted by aerosol absorption, yielding a larger aerosol index (de Graaf et al., 2005; Torres et al., in press, 2007).

Also clearly shown in Fig. 2 is that AOD and AI relationships depend strongly on aerosol type. For a specific cloud optical depth range, the AOD/AI ratio in the dust outflow region is much higher than that in the smoke outflow region. Fig. 4a shows the AOD₅₃₂/AI ratio as a function of LN(COD), a proxy for cloud albedo. For both smoke and dust, the AOD₅₃₂/AI ratio correlates with cloud albedo nearly linearly (with correlation coefficient R² of more than 0.98). The regression equations are also denoted in the figure. It appears that the dependence of AOD₅₃₂/AI ratio on COD for dust is about a factor of 2 larger than that for smoke. As discussed in Section 3.1, CALIOP AOD is lower than MODIS AOD by different magnitudes in the smoke and dust outflow regions. After potential MODIS AOD bias is reduced, MODIS AOD is 67% higher than CALIOP AOD in the smoke outflow region (i.e., MODIS/CALIOP AOD ratio = 1.67). While in the dust outflow region, MODIS AOD is 23% lower than CALIOP AOD (i.e., MODIS/CALIOP AOD ratio = 0.77). A simple scaling of CALIOP AOD using the above MODIS/CALIOP ratios yields that the COD-dependence of AOD₅₃₂/AI ratio differs by no more than 10% for smoke and dust, as illustrated in Fig. 4b.

To better understand factors determining the ratio between AOD and AI, we further account for the wavelength difference between CALIOP AOD (at 532 nm) and OMI AI (using the 352–388 nm pair) measurements. Dust and smoke differ substantially in size distributions and hence the wavelength-dependence of extinction. If an Angstrom exponent of 1.5 and 0.3 over the 388–532 nm spectral range is assumed for smoke and dust respectively (Eck et al., 1999), we can get AOD₃₈₈/AI ratio as function of ln(COD) by scaling Fig. 4b with a respective scaling factor of 1.56 and 1.10, as shown in Fig. 4c. For a given COD, the AOD₃₈₈/AI ratio for the smoke turns out to be 35–55% higher than that for the dust. This difference in the AOD₃₈₈/AI ratio between smoke and dust is qualitatively consistent with observed differences between smoke and dust in both the magnitude and spectral variation of absorption in the UV range. While the single-scattering albedo for smoke aerosol remains a nearly constant value of 0.89 in the UV

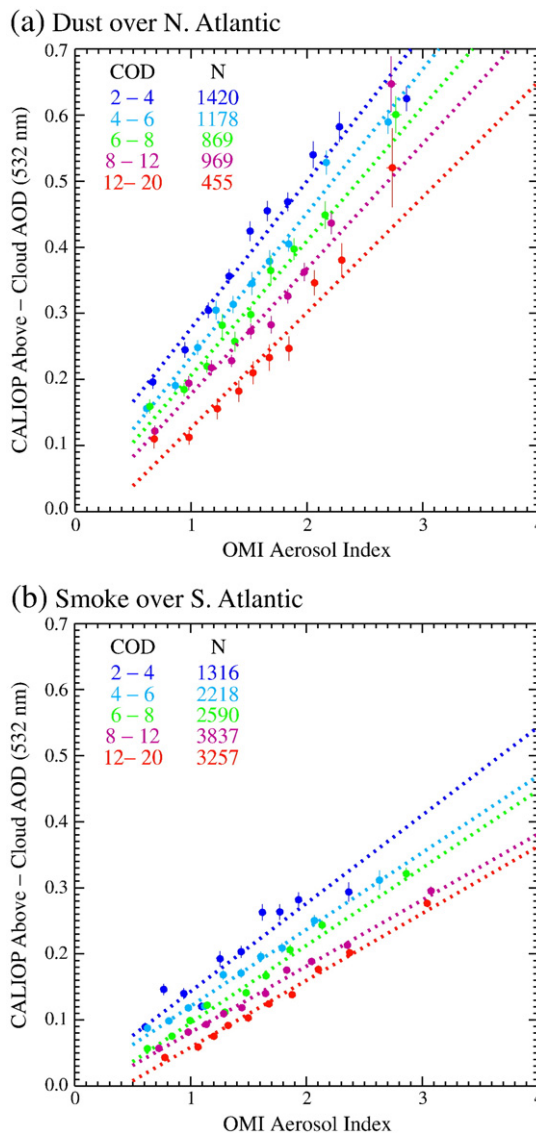


Fig. 2. Relationships between above-cloud AOD and aerosol index as a function of cloud optical depth (COD) for (a) dust over North Atlantic and (b) smoke over South Atlantic. Five COD groups are indicated by colors. In each COD group, the number of data entries is N (as listed in the legend) and all the data points are sorted by AI and arranged into 10 AI bins with equal data entries. Vertical and horizontal bar indicates standard error of AOD and aerosol index, respectively. Dotted lines represent a linear fit of data points for individual COD ranges. (For interpretation of the references to color in this figure legend, the reader is referred to the web version of this article.)

range, the dust single-scattering albedo increases from about 0.80 at 352 nm to about 0.83 at 388 nm (Bergstrom et al., 2007; Russell et al., 2010). Aerosol index increases with increasing absorption or decreasing aerosol single-scattering albedo (Torres et al., 1998). An increase of aerosol single-scattering albedo with wavelength in the UV (i.e., stronger absorption in shorter wavelength, such as for dust) can also raise the AI value (de Graaf et al., 2005). Therefore, the differences in single-scattering albedo between dust and smoke would yield a higher AI value and hence smaller AOD₃₈₈/AI ratio in the dust outflow region than in the smoke outflow region.

Several other factors would also contribute to the AOD–AI relationships. As shown in Fig. 3 and Table 1, the aerosol–cloud distance is more or less the same in the dust and smoke outflow region and should not be a reason for the observed regional difference in AOD/AI ratio. AI values also depend on observation geometry. While the viewing zenith angle for OMI is about 32° in both regions, the mean solar zenith angle of 38.5° in the smoke outflow region is larger than 25.3° in the dust

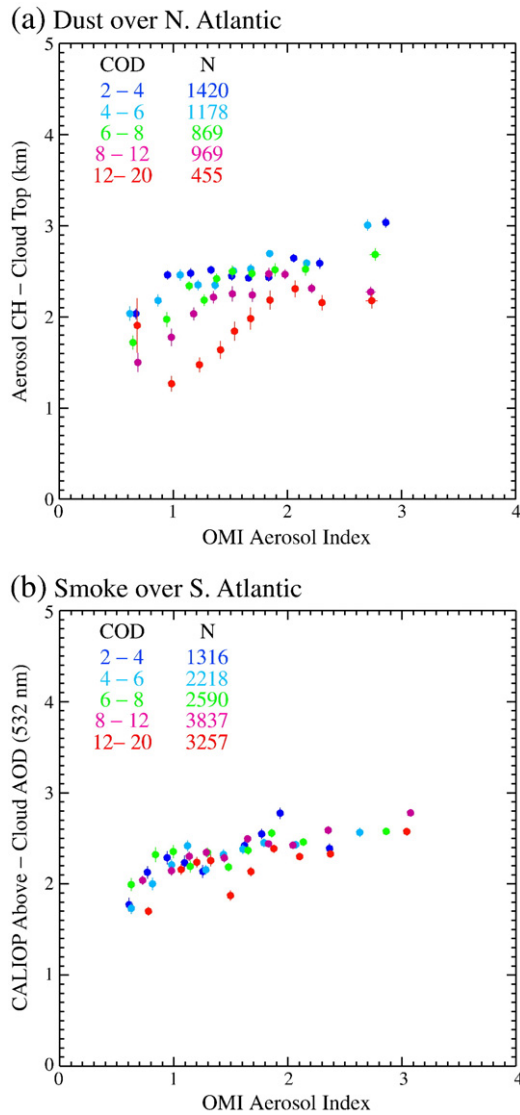


Fig. 3. Change of the aerosol–cloud distance (= aerosol centroid height CH – cloud top height) with aerosol index in 5 cloud optical depth (COD) groups for (a) dust over North Atlantic and (b) smoke over South Atlantic. The data are grouped into COD and AI bins. Vertical and horizontal bar indicates standard error of the aerosol–cloud distance and aerosol index, respectively. (For interpretation of the references to color in this figure legend, the reader is referred to the web version of this article.)

outflow region (Table 1). Such difference in the solar zenith angle would result in a higher AI value (de Graaf et al., 2005) and hence a lower AOD/AI ratio in the smoke outflow region than in the dust outflow region. In addition, the presence of smoke above clouds could bias the MODIS cloud optical depth low because strong smoke absorption in the visible darkens the cloud (Haywood et al., 2004; Wilcox et al., 2009). The low bias in COD increases with increasing AOD. Therefore, the AOD/AI ratio for smoke has been biased low, especially at high AI range.

4. Concluding remarks

We have conducted an integrated analysis of above-cloud AOD and AI relationships as a function of cloud optical depth by using 8-months of A-Train measurements of aerosol and cloud properties in the Saharan dust outflow and Southwest African smoke outflow regions. The analysis shows that the above-cloud AOD₅₃₂ from CALIPSO lidar correlates positively with OMI AI in approximately a linear manner, with the AOD₅₃₂/AI ratio decreasing with increasing cloud optical depth. The dependence of AOD–AI relationship on cloud optical depth is consistent with

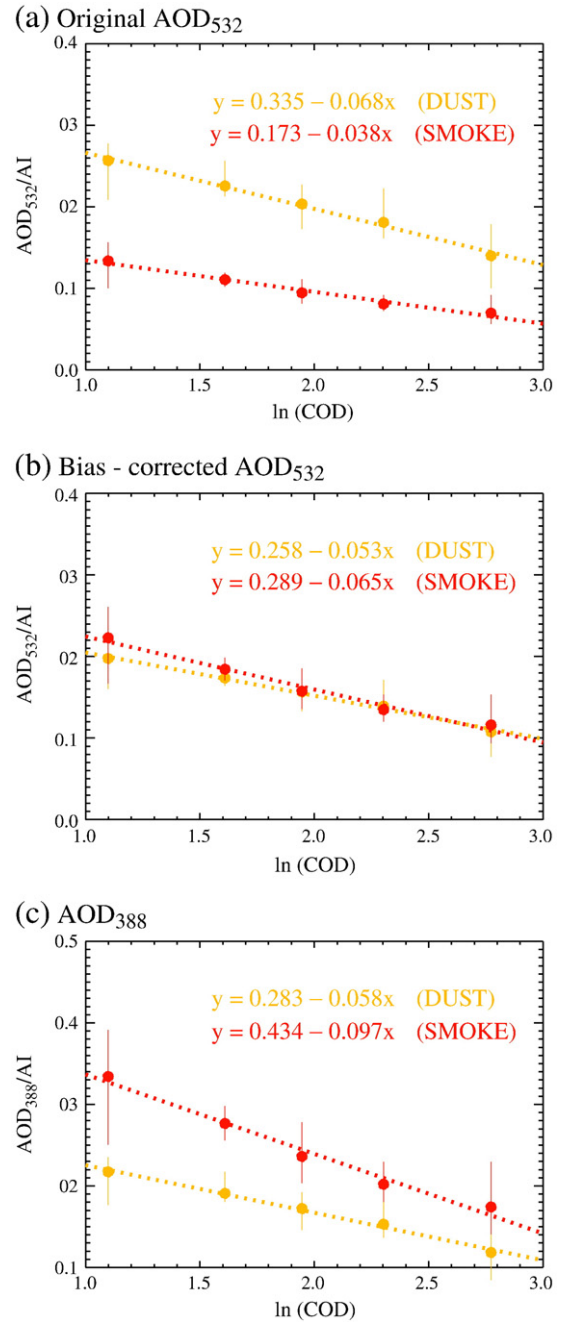


Fig. 4. Relationships between the AOD/AI ratio and ln(COD) for dust (orange) and smoke (red): (a) using original AOD (at 532 nm) from CALIOP, (b) correcting CALIOP AOD (at 532 nm) bias, and (c) correcting CALIOP AOD bias and extrapolating AOD from 532 nm to 388 nm (assuming an Angstrom exponent of 1.5 and 0.3 for smoke and dust, respectively). The average and range of AOD/AI ratio is represented as dot and vertical line, respectively. Linear fit to the average AOD/AI ratio is shown as dotted line, with the regression equation denoted. (For interpretation of the references to color in this figure legend, the reader is referred to the web version of this article.)

theoretical calculations that the multiple scattering by cloud decks enhances the interactions of aerosol absorption with UV radiation and raises the value of AI. The derived AOD₅₃₂/AI ratio doesn't depend on aerosol type when the potential biases in the CALIOP AOD measurements are empirically accounted for. However, the COD-dependence of AOD₃₈₈/AI ratio is different for smoke and dust, which is in general consistent with their differences in single-scattering albedo in the UV range.

The findings of our integrated analysis imply that the OMI aerosol index may be potentially used in conjunction with MODIS measurements of cloud optical depth and fraction to empirically derive the

above-cloud AOD for absorbing aerosols, such as dust and smoke, with a spatial coverage much more extensive than the CALIOP observations. A great deal of effort is needed to further explore the feasibility of this empirical approach. Current analysis deals only with cloudy OMI pixels (with cloud fraction greater than 0.9). For partially cloudy OMI pixels, the analysis should also factor in clear-sky AOD measurements from MODIS (Remer et al., 2008) and MISR (Kahn et al., 2005). A suite of radiative transfer modeling is also needed to both interpret and extrapolate the observed empirical relationships between above-cloud AOD and AI and their dependence on cloud optical depth. Last but not the least, it is essential to reduce biases and uncertainties associated with CALIOP measurements because such an empirical approach will naturally inherit CALIOP AOD biases and uncertainties. Correcting the MODIS COD bias in the smoke outflow region also needs to be investigated, although the resultant uncertainties may be partially canceled out through a consistent use of MODIS COD in the empirical approach. This empirical approach without assuming aerosol optical properties would complement the most recent effort of more robust retrieval of above-cloud AOD from OMI AI and radiance measurements (Torres et al., 2012).

Acknowledgments

The work was sponsored by NASA through its Radiation Science program, and Atmospheric Composition Modeling and Analysis Program (ACMAP), managed by Richard Eckman. We are grateful to Omar Torres, Tom Eck, Jeffery Reid, and Zhibo Zhang for helpful discussions. We thank three anonymous reviewers for comments. The MODIS data were obtained from the NASA Level 1 and Atmosphere Archive and Distribution System (LAADS). The OMI data were obtained from the NASA Goddard Earth Sciences Data and Information Services Center (GES DISC). The CALIPSO data were obtained from the NASA Langley Research Center Atmospheric Sciences Data Center.

References

- Abel, S. J., Highwood, H. J., Haywood, J. M., & Stringer, M. A. (2005). The direct radiative effect of biomass burning aerosols over southern Africa. *Atmospheric Chemistry and Physics*, 5, 1999–2018.
- Ahn, C., Torres, O., & Bhartia, P. K. (2008). Comparison of Ozone Monitoring Instrument UV aerosol products with Aqua/Moderate Resolution Imaging Spectroradiometer and Multiangle Imaging Spectroradiometer observations in 2006. *Journal of Geophysical Research*, 113, D16S27, doi:10.1029/2007JD008832.
- Anderson, T. L., Charlson, R. J., Winker, D. M., Ogren, J. A., & Holmen, K. (2003). Mesoscale variations of tropospheric aerosols. *Journal of Atmospheric Science*, 60, 119–136.
- Bergstrom, R. W., Pilewskie, P., Russell, P. B., Redemann, J., Bond, T. C., Quinn, P. K., et al. (2007). Spectral absorption properties of atmospheric aerosols. *Atmospheric Chemistry and Physics*, 7, 5937–5943.
- Cahalan, R. F., Ridgway, W., Wiscombe, W. J., Bell, T. L., & Snider, J. B. (1994). The albedo of fractal stratocumulus clouds. *Journal of Atmospheric Science*, 52, 2304–2316.
- Chand, D., Anderson, T. L., Wood, R., Charlson, R. J., Hu, Y., Liu, Z., et al. (2008). Quantifying above-cloud aerosol using spaceborne LiDAR for improved understanding of cloudy-sky direct climate forcing. *Journal of Geophysical Research*, 113, D13206, doi:10.1029/2007JD009433.
- Chand, D., Wood, R., Anderson, T. L., Satheesh, S. K., & Charlson, R. J. (2009). Satellite-derived direct radiative effect of aerosols dependent on cloud cover. *Nature Geoscience*, 2, 181–184, doi:10.1038/ngeo437.
- Christopher, S. A., Gupta, P., Haywood, J., & Greed, G. (2008). Aerosol optical thicknesses over North Africa: 1. Development of a product for model validation using Ozone Monitoring Instrument, Multiangle Imaging Spectroradiometer, and Aerosol Robotic Network. *Journal of Geophysical Research*, 113, D00C04, doi:10.1029/2007JD009446.
- de Graaf, M., Stamnes, P., & Aben, E. A. A. (2007). Analysis of reflectance spectra of UV-absorbing aerosol scenes measured by SCIAMACHY. *Journal of Geophysical Research*, 112, D02206, doi:10.1029/2006JD007249.
- de Graaf, M., Stamnes, P., Torres, O., & Koelemeijer, R. B. A. (2005). Absorbing Aerosol Index: Sensitivity analysis, application to GOME and comparison with TOMS. *Journal of Geophysical Research*, 110, D01201, doi:10.1029/2004JD005178.
- Devasthale, A., & Thomas, M. A. (2011). A global survey of aerosol–liquid water cloud overlap based on four years of CALIPSO–CALIOP data. *Atmospheric Chemistry and Physics*, 11, 1143–1154.
- Eck, T. F., Holben, B. N., Reid, J. S., Dubovik, O., Smirnov, A., O'Neill, N. T., et al. (1999). Wavelength dependence of the optical depth of biomass burning, urban and desert dust aerosols. *Journal of Geophysical Research*, 104, 31333–31350.
- Haywood, J. M., Osborne, S. R., & Abel, S. J. (2004). The effect of overlying absorbing aerosol layers on remote sensing retrievals of cloud effective radius and cloud optical depth. *Quarterly Journal of the Royal Meteorological Society*, 130, 779–800.
- Herman, J. R., Bhartia, P. K., Torres, O., Hsu, C., Sefort, C., & Celarier, E. A. (1997). Global distributions of UV-absorbing aerosols from NIMBUS 7/TOMS data. *Journal of Geophysical Research*, 102, 16911–16922 E. A..
- Hsu, N. C., Herman, J. R., Gleason, J. F., Torres, O., & Sefort, C. J. (1999a). Satellite detection of smoke aerosols over a snow/ice surface by TOMS. *Geophysical Research Letters*, 26, 1165–1168.
- Hsu, N. C., Herman, J. R., Torres, O., Holben, B. N., Tanre, D., Eck, T. F., et al. (1999b). Comparisons of the TOMS aerosol index with Sun-photometer aerosol optical thickness: Results and applications. *Journal of Geophysical Research*, 104, 6269–6279.
- Hsu, N. C., Herman, J. R., & Tsay, S. -C. (2003). Radiative impacts from biomass burning in the presence of clouds during boreal spring in southeast Asia. *Geophysical Research Letters*, 30, 1224, doi:10.1029/2002GL016485.
- Johnson, B. T., Shine, K. P., & Forster, P. M. (2004). The semi-direct aerosol effect: Impact of absorbing aerosols on marine stratocumulus. *Quarterly Journal of the Royal Meteorological Society*, 130, 1407–1422.
- Kahn, R. A., Gärtley, R., Martonchik, J., Diner, D., Crean, K., & Holben, B. N. (2005). MISR global aerosol optical depth validation based on two years of coincident AERONET observations. *Journal of Geophysical Research*, 110, D10S04, doi:10.1029/2004JD004706.
- Kahn, R. A., Garay, M. J., Nelson, D. L., Levy, R. C., Bull, M. A., Diner, D., et al. (2011). Response to “Toward unified satellite climatology of aerosol properties. 3. MOIS versus MISR versus AERONET”. *Journal of Quantitative Spectroscopy and Radiative Transfer*, 112, 901–909.
- Kittaka, C., Winker, D. M., Vaughan, M. A., Omar, A., & Remer, L. A. (2011). Intercomparison of column aerosol optical depths from CALIPSO and MODIS-Aqua. *Atmospheric Measurement Techniques*, 4, 131–141.
- Platnick, S., King, M. D., Ackerman, S. A., Menzel, W. P., Baum, B. A., Riedi, J. C., et al. (2003). The MODIS cloud products: Algorithms and examples from Terra. *IEEE Transactions on Geoscience and Remote Sensing*, 41, 459–473.
- Remer, L. A., Kaufman, Y. J., Tanre, D., Mattoo, S., Chu, D. A., Martins, J. V., et al. (2005). The MODIS aerosol algorithm, products and validation. *Journal of Atmospheric Science*, 62, 947–973.
- Remer, L. A., Kleidman, R. G., Levy, R. C., Kaufman, Y. J., Tanre, D., Mattoo, S., et al. (2008). Global aerosol climatology from the MODIS satellite sensors. *Journal of Geophysical Research*, D14S07, 113, doi:10.1029/2007JD009661.
- Russell, P. B., Bergstrom, R. W., Shinozuka, Y., Clarke, A. D., DeCarlo, P. F., Jimenez, J. L., et al. (2010). Absorption Angstrom Exponent in AERONET and related data as an indicator of aerosol composition. *Atmospheric Chemistry and Physics*, 10, 1155–1169.
- Schulz, M., Textor, C., Kinne, S., Balkanski, Y., Bauer, S., Bernsten, T., et al. (2006). Radiative forcing by aerosols as derived from the AeroCom present-day and pre-industrial simulations. *Atmospheric Chemistry and Physics*, 6, 5225–5246.
- Shi, Y., Zhang, J., Reid, J. S., Holben, B. N., Hyer, E. J., & Curtis, C. (2011). An analysis of the collection 5 MODIS over-ocean aerosol optical depth product for its implication in aerosol assimilation. *Atmospheric Chemistry and Physics*, 11, 557–565.
- Stephens, G. L., Vane, D. G., Boain, R. J., Mace, G. G., Sassen, K., Wang, Z., et al. (2002). The CloudSat mission and the A-Train: A new dimension of space-based observation of clouds and precipitation. *Bulletin of the American Meteorological Society*, 83, 1771–1790.
- Textor, C., Schulz, M., Guibert, S., Kinne, S., Balkanski, Y., Bauer, S., et al. (2006). Analysis and quantification of the diversities of aerosol life cycles within AeroCom. *Atmospheric Chemistry and Physics*, 6, 1777–1813.
- Torres, O., Bhartia, P. K., Herman, J. R., Ahmad, Z., & Gleason, J. (1998). Derivation of aerosol properties from satellite measurements of backscattered ultraviolet radiation: Theoretical basis. *Journal of Geophysical Research*, 103, 17,099–17,110.
- Torres, O., Jethva, H., & Bhartia, P. K. (in press). Retrieval of aerosol optical depth over clouds from OMI observations: Sensitivity analysis and case studies. *Journal of Atmospheric Science*, doi:10.1175/JAS-D-11-0130.1.
- Torres, O., Tanskanen, A., Veihelmann, B., Ahn, C., Braak, R., Bhartia, P. K., et al. (2007). Aerosols and surface UV products from Ozone Monitoring Instrument observations: An overview. *Journal of Geophysical Research*, 112, D24S47, doi:10.1029/2007JD008809.
- Waquet, F., Riedi, J., Labonnote, C., Goloub, P., Cairns, B., Deuze, J. -L., et al. (2009). Aerosol remote sensing over clouds using A-Train observations. *Journal of Atmospheric Science*, 66, 2468–2480.
- Wilcox, E. M. (2010). Stratocumulus cloud thickening beneath layers of absorbing smoke aerosol. *Atmospheric Chemistry and Physics*, 10, 11769–11777.
- Wilcox, E. M., Harshvardhan, & Platnick, S. (2009). Estimate of the impact of absorbing aerosol over cloud on the MODIS retrievals of cloud optical thickness and effective radius using two independent retrievals of liquid water path. *Journal of Geophysical Research*, 114, D05210, doi:10.1029/2008JD010589.
- Winker, D. M., Pelon, J., Coakley, J. A., Jr., Ackerman, S. A., Charlson, R. J., Colarco, P. R., et al. (2010). The CALIPSO mission: A global 3D view of aerosols and clouds. *Bulletin of the American Meteorological Society*, 91, 1211–1229.
- Winker, D. M., Vaughan, M. A., Omar, A., Hu, Y., Powell, K. A., Liu, Z., et al. (2009). Overview of the CALIPSO mission and CALIOP data processing algorithms. *Journal of Atmospheric and Oceanic Technology*, 26, 2310–2323, doi:10.1175/2009JTECHA1281.1.
- Yu, H., Chin, M., Winker, D. M., Omar, A. H., Liu, Z., Kittaka, C., et al. (2010). Global view of aerosol vertical distributions from CALIPSO lidar measurements and GOCART simulations: Regional and seasonal variations. *Journal of Geophysical Research*, 115, D00H30, doi:10.1029/2009JD013364.

- Yu, H., Kaufman, Y. J., Chin, M., Feingold, G., Remer, L. A., Anderson, T. L., et al. (2006). A review of measurement-based assessments of aerosol direct radiative effect and forcing. *Atmospheric Chemistry and Physics*, 6, 613–666.
- Yu, H., Remer, L. A., Chin, M., Bian, H., Kleidman, R. G., & Diehl, T. (2008). A satellite-based assessment of trans-Pacific transport of pollution aerosol. *Journal of Geophysical Research*, 113, D14S12, doi:10.1029/2007JD009349.
- Zhang, J., & Reid, J. S. (2006). MODIS aerosol product analysis for data assimilation: Assessment of over-ocean level 2 aerosol optical thickness retrievals. *Journal of Geophysical Research*, 111, D22207, doi:10.1029/2005JD006898.
- Zhang, J., & Reid, J. S. (2009). An analysis of clear-sky and contextual biases using an operational over ocean MODIS aerosol product. *Geophysical Research Letters*, 36, L15824, doi:10.1029/2009GL038723.